Biosensors and Bioelectronics 254 (2024) 116224

Contents lists available at ScienceDirect

Biosensors and Bioelectronics

journal homepage: www.elsevier.com/locate/bios

Monitoring the electroactive cargo of extracellular vesicles can differentiate various cancer cell lines

Chloe L. Miller [a,b], Mareike Herrmann [a,b], David R.F. Carter [c], Nicholas Turner [d], Priya Samuel [c], Bhavik Anil Patel [a,b,*]

[a] School of Applied Sciences, Italy
[b] Centre for Lifelong Health, University of Brighton, Brighton, BN2 4GJ, UK
[c] Department of Biological and Medical Sciences, Faculty of Health and Life Sciences, Oxford Brookes University, OX3 0BP, UK
[d] Department of Chemistry, University of Sheffield, Sheffield, S3 7HF, UK

ARTICLE INFO

Keywords:
Extracellular vesicles
Cancer
Microelectrodes
Single entity electrochemistry

ABSTRACT

Extracellular vesicles (EVs) are pivotal in cell-to-cell communication due to the array of cargo contained within these vesicles. EVs are considered important biomarkers for identification of disease, however most measurement approaches have focused on monitoring specific surface macromolecular targets. Our study focuses on exploring the electroactive component present within cargo from EVs obtained from various cancer and non-cancer cell lines using a disk carbon fiber microelectrode. Variations in the presence of oxidizable components were observed when the total cargo from EVs were measured, with the highest current detected in EVs from MCF7 cells. There were differences observed in the types of oxidizable species present within EVs from MCF7 and A549 cells. Single entity measurements showed clear spikes due to the detection of oxidizable cargo within EVs from MCF7 and A549 cells. These studies highlight the promise of monitoring EVs through the presence of varying electroactive components within the cargo and can drive a wave of new strategies towards specific detection of EVs for diagnosis and prognosis of various diseases.

1. Introduction

Extracellular vesicles (EVs) are heterogenous, nanoscale phospholipid vesicles which are actively secreted by all mammalian cells and have been identified as mediators of cell-to-cell communication (Couch et al., 2021). Similar sized EVs can be further classified based on their biogenesis, size, and biophysical properties. EVs contain a host of important communication cargo, such as proteins, metabolites, RNAs, DNAs and lipids. Due to their stability and presence in most bodily fluids and resemblance of their contents to the parental cell, EVs have been considered as important vehicles of intercellular communication and circulating biomarkers for disease diagnoses and prognosis. This makes EVs are highly attractive as a liquid biopsy biomarker for various diseases and has particularly been the focus for early detection of cancer (Pink et al., 2022; Wang et al., 2022; Yu et al., 2021).

A host of different single entity analytical detection techniques, mainly based on optical and electrochemical approaches have been established to identify EVs as biomarkers for disease detection (Bagheri Hashkavayi et al., 2020; Dezhakam et al., 2023; Jia et al., 2022; Welsh et al., 2023). Most electrochemical single entity approaches have focused on the determination of the intact EV and specific surface structures. Studies using electrical biosensors have focused on monitoring changes in the current due to the interaction of the EV on a polarized electrode surface, which provided a means to determine size and number of EVs. Electrochemical biosensors have predominately focused on the modification of the electrode with specific molecular tags such as aptamers (Boriachek et al., 2018; Zhang et al., 2021; Zhou et al., 2016), molecularly imprinted polymers (Zhu et al., 2020) and antibodies (Li et al., 2017; Li and Ma, 2022; Yadav et al., 2017) for the identification of surface markers for specific detection of a population of EVs, such as those from tumor cells. Very few single entity studies have focused on monitoring the internal cargo, in which an electric field is utilized to rupture the membrane of the EV allowing for the release of the internalized molecules (Li and Ma, 2022; Luo et al., 2020). Within such studies, simultaneous disruption and detection of released exosomal RNA/proteins have been conducted (Lin et al., 2020; Taller et al., 2015), but no other components have been accessed.

Studies of the internal cargo of EVs have been widely conducted,

* Corresponding author. Centre for Lifelong Health, University of Brighton, Brighton, BN2 4GJ, UK.
E-mail address: b.a.patel@brighton.ac.uk (B.A. Patel).

https://doi.org/10.1016/j.bios.2024.116224
Received 20 December 2023; Received in revised form 29 January 2024; Accepted 12 February 2024
Available online 19 March 2024

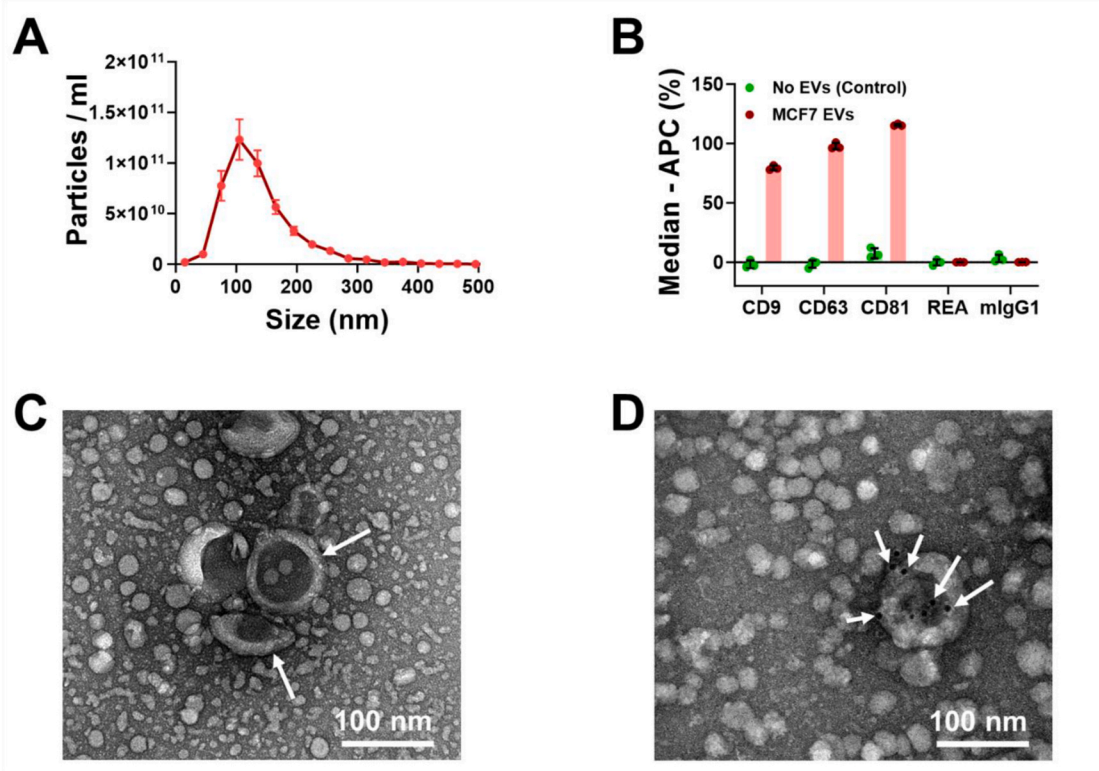

Fig. 1. Characterisation of EVs isolated from MCF-7 cells. (A) The graph shows the size distribution of EVs derived from MCF-7 breast cancer cells as determined by nanoparticle tracking analysis. The average total concentration of EVs in the samples was $4.5x10^{11} \pm 1.98x10^{11}$ particles/ml, where n = 9. (B) MACSPlex assay was performed to profile surface proteins on EVs. EVs were incubated overnight with MACSPlex immunocapture beads which comprise several poulations of variously fluorescently labelled beads each of which are coated with an antibody specific to a surface epitope on EVs or an isotype control; they were then labelled with APC conjugated cocktail of three antibodies against CD81/CD9/CD63. The graph shows histograms of relative median fluorescence intensity of CD81, CD9 and CD63 along with negative controls REA and mIgG1, where n = 3 and error bars represent Standard Deviation. (C) Transmission electron microscopy image of MCF-7 EVs negatively stained with 2% uranyl acetate. The white arrows point to some of the characteristic cup shaped EVs. (D) Transmission electron microscopy image of MCF-7 EVs immunolabelled with 10 nm gold particles conjugated antibodies to CD81 and then negatively stained with 2% uranyl acetate. The white arrows point to gold particles on the surface of EVs.

primarily focusing on proteins and nucleic acid contents (Bister et al., 2020; O'Brien et al., 2020; Qiu et al., 2019). However recently metabolomic studies of EVs have shown that the EV metabolome is an important source for biomarker discovery (Dudzik et al., 2021; Guan et al., 2021; Harmati et al., 2021; Puhka et al., 2017). Studies have highlighted a host of small organic molecules (such as amino acids, amines, fatty acids, carbohydrates, carbonic acids and purines) present from EVs obtained in vivo, ex vivo and from single cells (Puhka et al., 2017; Saito et al., 2021). Importantly, some of these metabolomic small organic molecules present within EV cargo which can be easily oxidised (Guan et al., 2021; Puhka et al., 2017), making them suitable to monitor using electrochemical techniques. Small molecules such as amines and certain amino acids like tryptophan have been shown to be easily oxidised directly on carbon fiber electrodes (Ou et al., 2019; Schapira et al., 2023). Single entity electrochemistry has been shown to be an effective approach to monitor the contents of vesicles and liposomes (Hu et al., 2023; Lebègue et al., 2015; Li et al., 2015; Zhang et al., 2017), where studies have monitored the total content of neurotransmitters present within vesicles (Omiatek et al., 2010). Such approaches can be suitable to explore if oxidizable cargo is present within EVs and if this varies between EVs obtained from different cell lines and diseases.

Within this study we present the electrochemical response of EVs obtained from a host of different cancerous and non-cancerous cell lines. Studies were conducted to monitor the total oxidizable cargo and monitor the cargo of individual EVs using single entity electrochemistry. Measurements were conducted using amperometry using a carbon fiber disc microelectrode. EVs were obtained from a host of different cell lines to compare if the oxidizable content varied. EVs were extracted from non-cancer cell lines (HME-hTert1 and HEK293), breast cancer cell lines (MCF-7 and BT-474), a gastric cancer cell line (HGC-27), a colorectal cancer cell line (SW480) and a lung cancer cell line (A549).

2. Materials and methods

2.1. Isolation and characterisation of extracellular vesicles from cell lines

Cell lines were grown in appropriate media as follows – Breast cancer cell lines: MCF-7 – DMEM/F-12 (Fisher); BT-474 – RPMI1640 supplemented with 10 g/mL insulin; lung cancer A549 – DMEM High glucose (SLS); colorectal cancer - SW480 - McCoy's 5a (Sigma-Aldrich); gastric cancer: HGC-27 – EMEM (Fisher) supplemented with 1 % Non-Essential Amino Acids (Fisher) and non-cancer cell lines: HME-hTert1 – DMEM/F-12 supplemented with 20 ng/mL EGF, 10 g/ml insulin (Sigma-Aldrich), and 100 g/ml hydrocortisone (Sigma-Aldrich) and HEK293 – DMEM High glucose (SLS). All media were further supplemented with 10 % fetal calf serum (Fisher) and 2.5 mM L-glutamine (Fisher). For EV depleted serum, foetal calf serum was centrifuged at 120,000 g for 16 h; the supernatant was carefully transferred to another tube and filtered through a 0.22 μm syringe filter. For EV depleted medium, 10 % fetal calf serum was replaced with 5% EV depleted fetal calf serum.

Cells were grown in EV depleted medium for 48 h. Conditioned media was serially centrifuged at 300 g × 5 min and 16,000 g × 20 min. The filtrate was concentrated down to 500 μL using 100 kDa vivaspin columns (Fisher). Size exclusion chromatography columns were

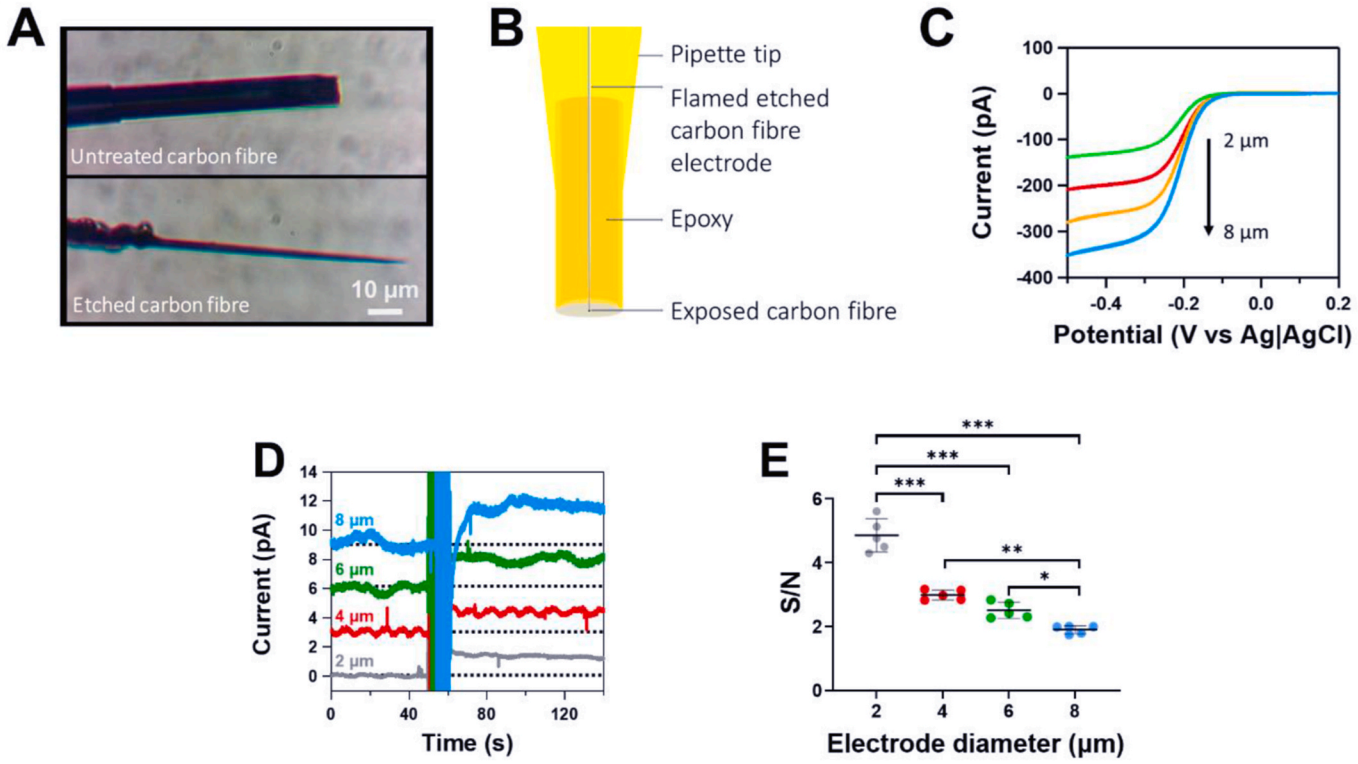

Fig. 2. Fabrication and characterisation of tuneable carbon fibre disk microelectrodes for measurement of extracellular vesicles (EVs). (A) shows optical microscopy images of protruding tip (7 µm carbon fiber electrode) which was flame etched to provide tuneable diameters. (B) schematic of the electrode, where the flame etched electrode was embedded within epoxy resin and cut using a diamond saw and polished to reveal a carbon fiber disc electrode and (C) shows cyclic voltammograms in ruthenium hexaamine for microelectrodes varying from 2 to 8 µm electrode diameter. (D) Comparing the signal to noise ratio for measurements of total cargo from EVs obtained from MCF7 cells. Amperometric measurements were conducted +750 mV vs Ag|AgCl on electrodes of varying diameter, where at 50 s, 1 mM Triton X surfactant was added to expose the cargo of the EVs. Dashed black line indicates the baseline. (E) Overall responses of the signal to noise ratio (S/N). Where data is shown as mean ± S.D., n = 5, *p < 0.05, **p < 0.01 and ***p < 0.001.

prepared with 14 mL of sepharose CL-2B (Fisher) slurry columns topped up with PBS. The column was then washed thrice with PBS before the sample was run and fractions of 500 µL were collected; fractions 6–10 were pooled to give the EV fractions. This was then concentrated down to 200 µL using ivaspin 5 kDA columns (VWR 10723837). EV number and size were assessed using ZetaView® by Particlemetrix using the manufacturer's instructions. The EV fractions were diluted to optimal concentrations ranging from 1:10,000 to 1:100,000 in PBS and loaded into the flow cell. Videos were taken at 11 positions; EV number and size were estimated from this using the zetaview software.

2.2. Fabrication of tuneable carbon fiber microelectrodes

The fabrication of the flame etched microelectrode was based on a method previously described by Ewing. Briefly, a 10 µm carbon fiber was aspirated into a borosilicate glass capillary (1.2 mm o.d., 0.69 mm i.d., Sutter Instrument Co., Novato, CA). The glass capillary was subsequently pulled into two separate electrodes with a commercial micropipette puller (model PE-21, Narishige, Inc., Japan). The fiber extending from the glass was cut to 100–150 µm with a scalpel under a microscope. To flame etch the carbon fiber, the electrodes were held on the edge of the blue part of a butane flame (Multiflame AB, Hässleholm, Sweden) for less than 2 s. As the end of the tip became red, the electrode was rotated in to ensure even etching. The resultant electrode was placed into a pipette tip and fully sealed with epoxy (Robnor Resins Ltd, UK) and left to set for 48 h at ambient room temperature. The electrode was then cut using a diamond wafer blade (Buehler saw). Lastly the electrode was polished sequentially in 1-, 0.3- and 0.05-µm alumina slurry. Only electrodes showing good reaction kinetics and a steady-state diffusion limited current were used for the experiments. To tailor the diameter of the disc electrode, the steady state limiting current was obtained following measurements in 1 mM ruthenium (III) hexamine in 1M KCl. The electrode was then further polished and re-ran using 1 mM ruthenium (III) hexamine in 1M KCl until the desired diameter was reached.

2.3. Electrochemical measurements of extracellular vesicles

Electrochemical measurements were carried out using CHI760 potentiostat (CH instruments, Texas) monitored using CHI software. All electrochemical measurements were carried out in the conventional three electrode configuration consisting of Ag|AgCl (3 M KCl) reference electrode, Pt wire counter electrode and a 2 µm diameter disc carbon fiber microelectrode as working electrode. Experimental set-up for measurements is shown on Fig. S1. Prior to conducting EV measurements, electrodes were run in Dulbecco's phosphate-buffered saline (DPBS), where, if the noise was within 2–5 x 10^{-13} A, then then electrode was utilized for measurements. Other than for studies to explore the variation of voltage on the current observed, all measurements were conducted at +750 mV vs Ag|AgCl, as many small organic metabolites that have been highlighted from metabolomic studies have been shown to be oxidised (Ou et al., 2019). For total measurements of EV cargo, measurements were conducted using 1 x 10^{-10} EVs in 1 mL of DPBS at room temperature (~21 °C). After recording the current baseline, at 50 s, 1 mM Triton X was added to burst all the EVs, and the current was recorded for a 90 s. The difference in the current observed from 0 to 20 s and 120–140 s was monitored. For single entity measurements, measurements were conducted using 1 x 10^{-10} EVs in 1 mL of DPBS, where amperometric recordings were monitored for 100 s in the presence of

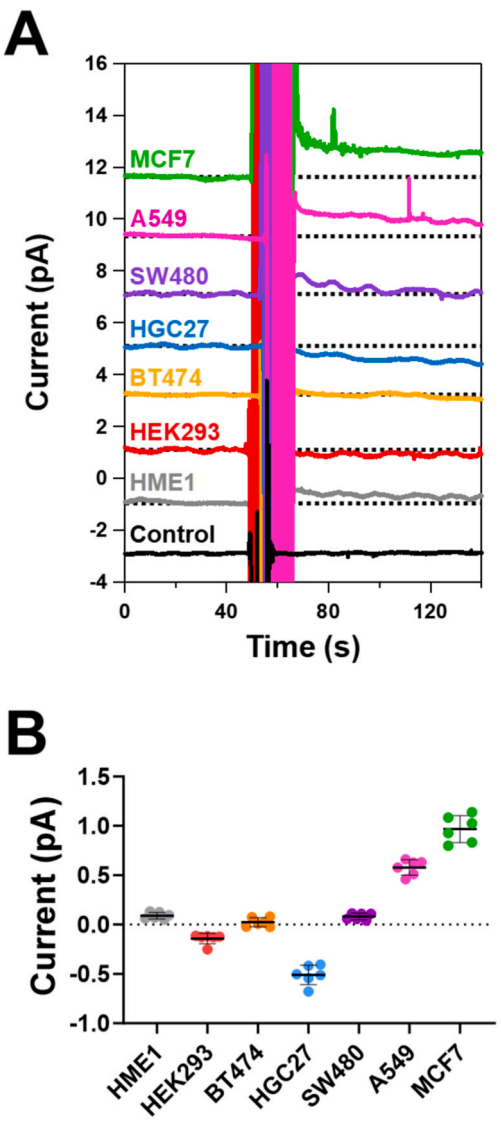

Fig. 3. Differences between EVs from cancerous and non-cancerous cells. (A) Amperometric measurements were conducted +750 mV vs Ag|AgCl, where at 50 s, 1 mM Triton X surfactant was added to expose the cargo of the EVs. (B) The difference in the current observed from 0 to 20 s and 120–140 s was taken from multiple measurements, where clear differences in the current were obtained between different EVs. In all cases, measurements were conducted using 1 x 10^{10} EVs. Dashed black line indicates the baseline. Where data is shown as mean ± S.D., n = 6.

100 μM Triton X. The peak amplitude of individual spikes was monitored.

2.4. Chromatographic measurements of extracellular vesicles

The HPLC system consisted of a Jasco pump (Model PU-2080), a Rheodyne manual injector with a 20 μL loop and a kinetic ODS 2.6 μm 100 mm × 2.1 mm i.d. analytical column with a guard column. The HPLC system was used in a completely isocratic mode for the determination of signalling metabolites and set at a flow rate of 100 μL min^{-1}. A dual 3 mm glassy carbon electrode (BASi) served as the working electrodes and was used with an Ag|AgCl reference electrode and a stainless-steel auxiliary block as the counter electrode. The working electrodes were set at potentials of +950 mV and +650 mV vs the Ag|AgCl reference electrode. Detector voltage and recording current was regulated by the CHI802D potentiostat (CH Instruments, Texas, USA). CHI802D software was used for data collection and processing. A cyclic voltammetry pre-treatment run (2 cycles of −2.5 V to +2.5 V at 0.1 V/s) was used between each sample to eliminate any effects of fouling.

The stock buffer for the mobile phase was comprised of the following: 0.1 M sodium acetate, 0.1 M citric acid, and 27 μM disodium ethylene–diamine–tetra-acetate (EDTA) dissolved in 1 L of deionized, reverse osmosis water (RO H_2O) and buffered to pH 3.0 using concentrated hydrochloric acid. To prepare the mobile phase, the HPLC grade methanol (Fisher Scientific) was mixed with the stock buffer in a ratio of 12:88 (v/v) and degassed after mixing. For EV analysis, 50 μL of 0.1 M perchloric acid was added to 1 x 10^{10} EV from MCF-7 and A549 cells and centrifuged at 13,200 g at 4 °C for 3 min. The resulting supernatant was then pushed through a 0.2 μm filter and measured.

3. Results and discussion

3.1. Isolation and characterization of extracellular vesicles

EVs from all cell lines were extracted using size exclusion columns. Fig. 1 shows the characterisation of EVs isolated from MCF-7 cells according to the MISEV guidelines (Théry et al., 2018). Fig. 1A NTA analysis was performed to estimate the particle size distribution of the derived EVs, where the maximum concentration was observed at ~100 nm. Transmission electron microscopy of MCF-7 EVs (Fig. 1B) negatively stained with 2% uranyl acetate showed characteristic cup-shaped EVs with diameter ranging from ~30 nm to ~230 nm with an average size of 74.8 nm. Immunogold labelling of MCF-7 EVs with anti CD81 antibodies (Fig. 1C) shows gold particles adherent to the surface of the EVs. MACSPlex analysis was performed where EVs are incubated with a mix of populations of beads coated with specific antibodies to surface epitopes seen on EVs; fluorescence based flowcytometry then allows confirmation of the presence of EV markers on the surface of the particles. MACSPlex analysis of MCF-7 EVs (Fig. 1D) shows presence of tetraspannin markers – CD9, CD63 and CD81 – commonly found on the surface membrane of EVs. These characterisation studies using EVs isolated from MCF-7 cells showcase our ability to isolate extracellular vesicles for monitoring the internalized cargo and thus these approaches were utilized for various cell lines explored within this study.

3.2. Tuneable carbon fiber microelectrodes provide scope for total and individual measurements of extracellular vesicles

At present, measurements of the internal cargo are conducted mainly using vesicles which contain a high content of easily oxidizable neurotransmitters, using either disk or nanotip electrodes (Hu et al., 2023; Li et al., 2015; Phan et al., 2017), which have a large surface area for measurement. However, given that most of the cargo within EVs is not likely to be easily oxidised, we initially focused on optimising the surface area of the electrode to enhance the signal-to-noise ratio. To achieve this, we initially utilized the approach taken by Ewing to fabricate nanotip carbon fiber microelectrodes by flame etching (Dunevall et al., 2015; Hu et al., 2023) a 10 μm carbon fiber microelectrode (Fig. 2A). This flame-etched nanotip carbon fiber electrode was then cast in epoxy resin and slowly cut using a diamond saw to expose a disc electrode (Fig. 2B). Given the tapered nature of the flame-etched carbon fiber, following sequential polishing of the electrode surface, the active surface area of the electrode can be tuned to generate an electrode with dimensions suitable for any mode of electrochemical measurement. Fig. 2C shows cyclic voltammograms of ruthenium (III) hexamine, where the electrode diameter varied from 2 to 8 μm. This approach thus provides the means to generate disk electrode diameters from sub-micron to micron, which broadens the potential to enhance the sensitivity of carbon fiber microelectrodes. To explore the best electrode diameter for measurements, total cargo recordings were conducted using EVs obtained from MCF-7 cells as a model system for all other cell lines. The signal to noise ratio was compared for electrodes of varying

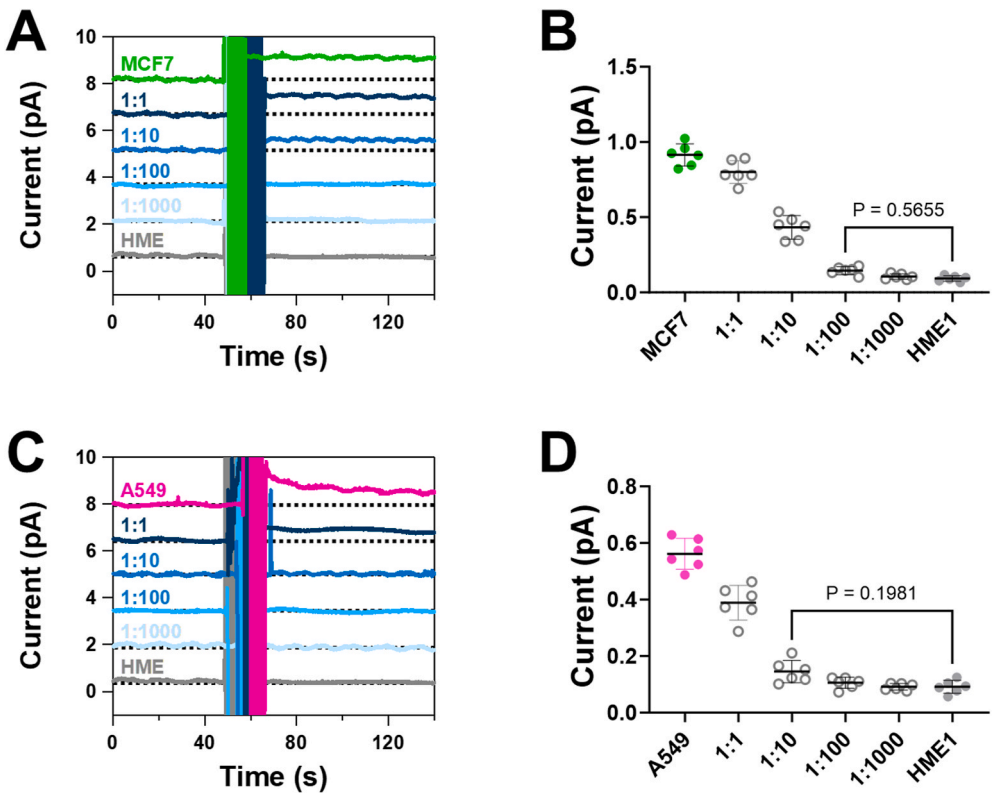

Fig. 4. Exploring the ability to detect cancerous EVs in the presence of non-cancerous EVs. A) Amperometric measurements were conducted +750 mV vs Ag|AgCl, where at 50 s, 1 mM Triton X surfactant was added to expose the cargo of the EVs from MCF7 cells. (B) The difference in the current observed from 0 to 20 s and 120–140 s was taken from multiple measurements for EVs from MCF7 cells. (C) Amperometric measurements were conducted +750 mV vs Ag|AgCl, where at 50 s, 1 mM Triton X surfactant was added to expose the cargo of the EVs from A549 cells. (B) The difference in the current observed from 0 to 20 s and 120–140 s was taken from multiple measurements for EVs from A549 cells. Dashed black line indicates the baseline. Where data is shown as mean ± S.D., n = 6.

diameter measurements (Fig. 2D). For all measurements, 2 μm diameter disc electrodes were utilized as they provided a significantly better signal to noise ratio for total cargo measurements when compared to electrodes with larger disc diameters (Fig. 2E).

3.3. Monitoring the total electroactive cargo within extracellular vesicles from different cancer cell lines

The first approach was to explore differences in the oxidizable cargo between different EVs through complete rupture of a large population of EVs. Fig. 3A shown amperometric traces, where the baseline current was recorded before the addition of 1 mM Triton X, which lysed the membrane of the EVs to expose the internal cargo. The difference in the current before and after the addition of Triton X was utilized to understand the amount of oxidizable cargo present. No difference in the current was observed when studies without EVs were conducted before and after the addition of Triton X. Fig. 3B shows that population data of EVs obtained from different cell lines. Minimal changes in the current were observed for EVs obtained from HME-hTert1, BT-474 and SW480 cells. This may be due to a lower fraction of electroactive cargo present within the EVs of these cell lines when compared to larger biomolecules (e.g. mRNA, DNA and proteins), or that the presence of electroactive cargo was below the detection capabilities of the electrode. Reductions in the observed current were observed in HEK293 and HGC27 EVs, suggestive that no oxidizable cargo is present. These reductions indicate that the cargo present within the EVs influenced the established charged double layer at the electrode surface, thus resulting in a reduced current response. Lastly, we observed positive current from EVs obtained from MCF7 and A549 cells. There was a significant difference ($p < 0.001$, $n = 6$) between the two breast cancer cell lines (MCF-7 and BT-474). These results highlight that even within a specific disease area, there can be variations in the electroactive cargo.

To gain an understanding in the responses observed from EVs from the different cell lines, measurements were conducted using different small organic compounds that have been highlighted from metabolomic studies (Dudzik et al., 2021; Harmati et al., 2021; Puhka et al., 2017). Fig. S2 shows that various small organic molecules (tryptophan, kynurenine, glutamic acid, norepinephrine, dopamine, and serotonin) can increase the current. Even though the concentration is identical, there is significant variation in the current observed. For two molecules, xanthine and adenosine, no differences were observed in the current. Lastly, there was a reduction in the current observed for kynurenic acid. Although some of these compounds may or may not be present within EVs detected within this study, our results clearly highlight that small organic compounds known to be identified in metabolomic studies can clearly alter the current response. Overall, the EVs obtained from different cell lines must contain a varied composition of electroactive cargo (most likely due to small organic molecules or access of oxidizable amino acids in peptides or proteins) which can provide significant promise in differentiating between different types of EVs.

3.4. Exploring the detection limit and long-term stability in monitoring the electroactive cargo of cancerous extracellular vesicles

Detecting the presence of specific EVs in a liquid biopsy has been seen to be a key approach towards the early diagnosis of varying diseases, particularly cancer. Therefore, we explored whether we could observe concentration dependency in the detection of EVs from MCF-7, which contained oxidizable compounds when present in different ratios with EVs from HME-hTert1. Fig. 4A shows there is a concentration dependent change in the current post exposure to Triton X. There is a clear relationship between the current observed and the concentration

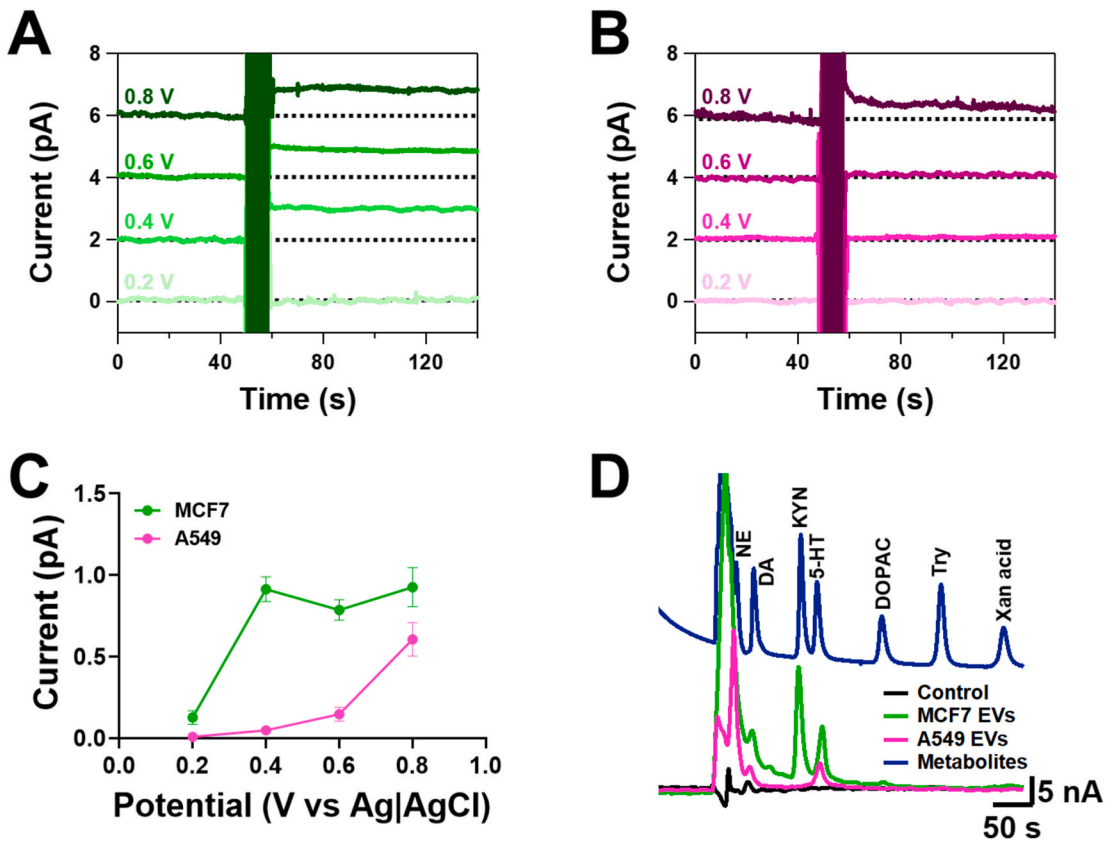

Fig. 5. Investigating if the oxidizable cargo within EVs varies. We explored the differences in the current over a range of voltages. Amperometric measurements were conducted +750 mV vs Ag|AgCl, where at 50 s, 1 mM Triton X surfactant was added to expose the cargo of EVs (A) from MCF-7 cells and (B) A549 cells. (C) Difference in the current observed from 0 to 20 s and 120–140 s was taken at different voltages. (D) Chromatogram obtained with an electrochemical detector for a range of metabolites and EV cargo obtained from MCF-7 and A549 cells. Dashed black line indicates the baseline. Where data is shown as mean ± S.D., n = 6.

of EVs from MCF-7 cells (Fig. 4B). There was no significant difference in the current when a 1:100 ratio is utilized when compared to EVs from HME-hTert1 alone ($p = 0.5655$, $n = 6$), demonstrating the detection limit for EVs from MCF-7 cells. In a similar approach measurement were conducted using EVs from A549 cells, where there was no difference in the current when a 1:10 ratio is utilized when compared to EVs from HME-hTert1 alone ($p = 0.1981$, $n = 6$). For EVs from A549, the detection limit was higher than that of MCF-7, due to the lower current observed. Enhancements could be achieved through specificity testing for electroactive cargo analytes using molecular recognition elements (e.g. aptamers and molecular conducting polymers) on electrochemical sensors.

The stability of EVs were explored by using EVs from MCF-7 cells, where measurements were conducted over different timescales for a month. Fig. S3 shows that that the current response did not vary when measurements were conducted up to 72 h. Post 72 h, there was a reduction in the current response, with an increase in the baseline current, where this was nearly identical following a month. These findings show a gradual reduction in the stability of the EVs, which allows the internalized cargo to be leached within the extracellular matrix and thus elevates the background current yielding to no distinction when Triton X was added to disrupt the membranes of the EVs. These findings highlight that for measurement of total cargo from EVs, studies should be conducted within 72 h.

3.5. Oxidizable components vary in the cargo of extracellular vesicles obtained from different cell lines

Only EVs from two cell lines (MCF-7 and A549) were shown to have oxidizable components within the cargo from the measurement in Fig. 3. However, it is not known if there is any differentiation in the electroactive cargo present. Amperometric measurements were obtained at varying voltages from MCF-7 (Fig. 5A) and A549 (Fig. 5B) EVs. The overall current responses are shown in Fig. 5C, where there is a clear difference in the current-voltage profiles, highlighting that the composition of oxidizable components present vary and the applied voltage can be used as a tool to selectively discriminate between different types of EVs. These current-voltage profiles may provide scope to discern and quantify specific electroactive components within EVs. To assess if the composition of substances were varied, chromatographic responses using an electrochemical detector were obtained, where differences in components were observed between EVs from MCF-7 and A549 cells (Fig. 5D). When compared with a mixture of small organic molecules, some of the peaks overlapped the compounds, indicative that electroactive amino acids like tryptophan and amines are most likely to present within EVs. These findings highlight the clear variations within the cargo of EVs, most likely due to the different metabolic profiles of EVs from different types of cancer, which have been supported from metabolomic studies (Guan et al., 2021; Harmati et al., 2021; Puhka et al., 2017), and that electrochemical approaches have real promise as detection tools of EV cargo.

3.6. Single entity electrochemical measurements of individual extracellular vesicular cargo

We explored the ability to conduct single-entity measurement of EVs from MCF-7 and A549 cells, which were both shown to have the greatest oxidizable cargo. The principle of single entity electrochemistry is shown in Fig. 6A, where the electrode is held at a voltage and the EVs adsorb onto the electrode surface and rupture, trapping their contents

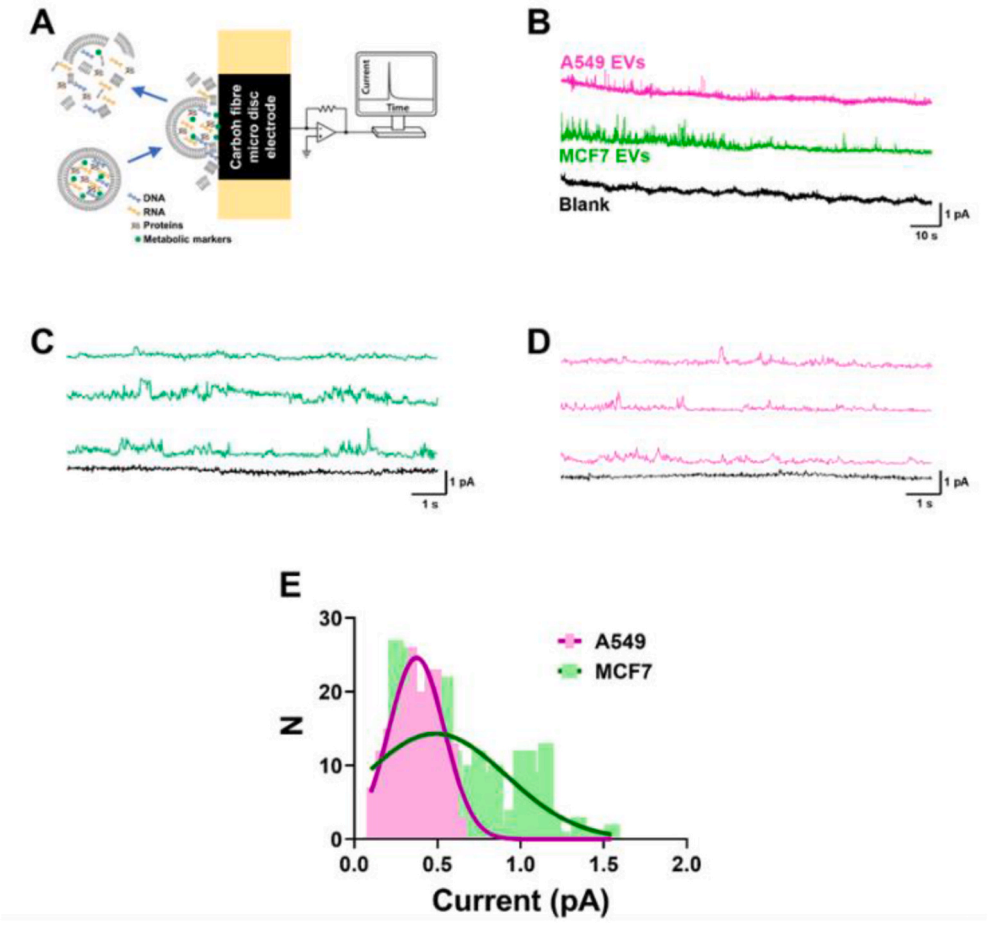

Fig. 6. Measurement of single EVs from MCF-7 and A549 cells. (A) shows schematic of the proposed experiment. (B) Responses from cancerous EVs and the black trace shows a control response where no EVs were present. Profile of individual spikes that represent the detection of individual EVs from (C) MCF-7 cells and (D) A549 cells. (E) Frequency distribution showing the peak current of the individual spikes from MCF-7 (n = 256) and A549 (n = 194) EVs. Measurements were carried out using a 2 μm diameter disc carbon fiber microelectrode where the electrode was held at +750 mV vs Ag|AgCl.

against the electrode. Studies conducted using quartz crystal microbalance highlighted this mechanism (Dimitrievski and Kasemo, 2008; Reimhult et al., 2009).

As the contents of each EV is oxidised, there is a sharp transient peak for each EV that bursts. Fig. 6B shows amperometric responses obtained from EVs from two cancer cell lines, where clear sharp spikes in the current were observed for MCF-7 (Fig. 6C) and A549 (Fig. 6D) EVs, which are due to individual vesicles bursting onto the electrode and the multiple oxidizable cargo being monitored at the electrode surface. This may explain the varying nature of peak shapes within our data, as each oxidizable component will have varying electron transfer kinetics on the carbon fiber electrode surface. The peak current amplitude of the individual spikes was monitored (n = 256 peaks for MCF-7 EVs and n = 194 for A549 EVs). The frequency distribution shown in (Fig. 6E) shows the presence of two different distributions for EVs from MCF-7 and A549 cells, which suggests that more oxidizable components are present in MCF-7 EVs when compared to A549 EVs. This finding indicates that within EVs from a single cell line there may be inherent heterogeneity with different vesicles containing different number of oxidizable substances. This is not surprising given that EVs represent a diverse range of vesicle sizes and composition. Our nanoparticle tracking analysis (Fig. 1A) shows the range of vesicle sizes varied from 50 to 500 nm. Therefore, these different distributions in the current observed in MCF-7 EVs could be due to different pools of vesicles.

4. Conclusions

In summary, we showcase for the first time that there is a varying presence of oxidizable substances within the cargo of EVs utilising amperometry with a tuneable carbon fiber microelectrode. The internalized cargo of EVs can be monitored by two approaches, firstly through the measurement of the total oxidizable cargo and secondly through measurements of individual EV cargo. The nature and amount of the oxidizable substances present within the cargo varies and thus provides further scope for differentiation. These key findings highlight that monitoring of electroactive internalized cargo can offer to identify specific types of EVs. These findings can help shape the development of new tools and technologies to monitor internalized cargo of EVs as vital biomarkers for diagnosis and prognosis.

CRediT authorship contribution statement

Chloe L. Miller: Writing – review & editing, Visualization, Validation, Methodology, Formal analysis, Data curation. **Mareike Herrmann:** Visualization, Validation, Methodology, Investigation, Formal analysis, Data curation. **David R.F. Carter:** Writing – review & editing, Supervision, Resources, Project administration, Funding acquisition, Conceptualization. **Nicholas Turner:** Writing – review & editing, Visualization, Validation, Funding acquisition, Conceptualization. **Priya Samuel:** Writing – original draft, Visualization, Validation, Resources, Project administration, Methodology, Investigation, Funding acquisition, Formal analysis, Data curation. **Bhavik Anil Patel:** Writing –

original draft, Visualization, Supervision, Resources, Project administration, Methodology, Funding acquisition, Formal analysis, Conceptualization.

Declaration of competing interest

The authors declare that they have no known competing financial interests or personal relationships that could have appeared to influence the work reported in this paper.

Data availability

Data will be made available on request.

Acknowledgements

The authors would like to acknowledge funding from CRUK/EPSRC.

Appendix A. Supplementary data

Supplementary data to this article can be found online at https://doi.org/10.1016/j.bios.2024.116224.

References

Bagheri Hashkavayi, A., Cha, B.S., Lee, E.S., Kim, S., Park, K.S., 2020. Advances in exosome analysis methods with an emphasis on electrochemistry. Anal. Chem. 92 (19), 12733–12740.

Bister, N., Pistono, C., Huremagic, B., Jolkkonen, J., Giugno, R., Malm, T., 2020. Hypoxia and extracellular vesicles: a review on methods, vesicular cargo and functions. J. Extracell. Vesicles 10 (1), e12002.

Boriachek, K., Islam, M.N., Möller, A., Salomon, C., Nguyen, N.-T., Hossain, M.S.A., Yamauchi, Y., Shiddiky, M.J.A., 2018. Biological functions and current advances in isolation and detection strategies for exosome nanovesicles. Small 14 (6), 1702153.

Couch, Y., Buzàs, E.I., Di Vizio, D., Gho, Y.S., Harrison, P., Hill, A.F., Lötvall, J., Raposo, G., Stahl, P.D., Théry, C., Witwer, K.W., Carter, D.R.F., 2021. A brief history of nearly EV-erything – the rise and rise of extracellular vesicles. J. Extracell. Vesicles 10 (14), e12144.

Dezhakam, E., Khalilzadeh, B., Mahdipour, M., Isildak, I., Yousefi, H., Ahmadi, M., Naseri, A., Rahbarghazi, R., 2023. Electrochemical biosensors in exosome analysis; a short journey to the present and future trends in early-stage evaluation of cancers. Biosens. Bioelectron. 222, 114980.

Dimitrievski, K., Kasemo, B., 2008. Simulations of lipid vesicle adsorption for different lipid mixtures. Langmuir 24 (8), 4077–4091.

Dudzik, D., Macioszek, S., Struck-Lewicka, W., Kordalewska, M., Buszewska-Forajta, M., Waszczuk-Jankowska, M., Wawrzyniak, R., Artymowicz, M., Raczak-Gutknecht, J., Siluk, D., Markuszewski, M.J., 2021. Perspectives and challenges in extracellular vesicles untargeted metabolomics analysis. TrAC, Trends Anal. Chem. 143, 116382.

Dunevall, J., Fathali, H., Najafinobar, N., Lovric, J., Wigström, J., Cans, A.-S., Ewing, A.G., 2015. Characterizing the catecholamine content of single mammalian vesicles by collision–adsorption events at an electrode. J. Am. Chem. Soc. 137 (13), 4344–4346.

Guan, F., Xiang, X., Xie, Y., Li, H., Zhang, W., Shu, Y., Wang, J., Qin, W., 2021. Simultaneous metabolomics and proteomics analysis of plasma-derived extracellular vesicles. Anal. Methods 13 (16), 1930–1938.

Harmati, M., Bukva, M., Böröczky, T., Buzás, K., Gyukity-Sebestyén, E., 2021. The role of the metabolite cargo of extracellular vesicles in tumor progression. Cancer Metastasis Rev. 40 (4), 1203–1221.

Hu, K., Le Vo, K.L., Wang, F., Zhang, X., Gu, C., Fang, N., Phan, N.T.N., Ewing, A.G., 2023. Single exosome amperometric measurements reveal encapsulation of chemical messengers for intercellular communication. J. Am. Chem. Soc. 145 (21), 11499–11503.

Jia, R., Rotenberg, S.A., Mirkin, M.V., 2022. Electrochemical resistive-pulse sensing of extracellular vesicles. Anal. Chem. 94 (37), 12614–12620.

Lebègue, E., Anderson, C.M., Dick, J.E., Webb, L.J., Bard, A.J., 2015. Electrochemical detection of single phospholipid vesicle collisions at a Pt ultramicroelectrode. Langmuir 31 (42), 11734–11739.

Li, Q., Tofaris, G.K., Davis, J.J., 2017. Concentration-normalized electroanalytical assaying of exosomal markers. Anal. Chem. 89 (5), 3184–3190.

Li, S., Ma, Q., 2022. Electrochemical nano-sensing interface for exosomes analysis and cancer diagnosis. Biosens. Bioelectron. 214, 114554.

Li, X., Majdi, S., Dunevall, J., Fathali, H., Ewing, A.G., 2015. Quantitative measurement of transmitters in individual vesicles in the cytoplasm of single cells with nanotip electrodes. Angew. Chem. Int. Ed. 54 (41), 11978–11982.

Lin, S., Yu, Z., Chen, D., Wang, Z., Miao, J., Li, Q., Zhang, D., Song, J., Cui, D., 2020. Progress in microfluidics-based exosome separation and detection technologies for diagnostic applications. Small 16 (9), 1903916.

Luo, L., Wang, L., Zeng, L., Wang, Y., Weng, Y., Liao, Y., Chen, T., Xia, Y., Zhang, J., Chen, J., 2020. A ratiometric electrochemical DNA biosensor for detection of exosomal MicroRNA. Talanta 207, 120298.

O'Brien, K., Breyne, K., Ughetto, S., Laurent, L.C., Breakefield, X.O., 2020. RNA delivery by extracellular vesicles in mammalian cells and its applications. Nat. Rev. Mol. Cell Biol. 21 (10), 585–606.

Omiatek, D.M., Dong, Y., Heien, M.L., Ewing, A.G., 2010. Only a fraction of quantal content is released during exocytosis as revealed by electrochemical cytometry of secretory vesicles. ACS Chem. Neurosci. 1 (3), 234–245.

Ou, Y., Buchanan, A.M., Witt, C.E., Hashemi, P., 2019. Frontiers in electrochemical sensors for neurotransmitter detection: towards measuring neurotransmitters as chemical diagnostics for brain disorders. Anal. Methods 11 (21), 2738–2755.

Phan, N.T.N., Li, X., Ewing, A.G., 2017. Measuring synaptic vesicles using cellular electrochemistry and nanoscale molecular imaging. Nat. Rev. Chem 1, 0048.

Pink, R.C., Beaman, E.-M., Samuel, P., Brooks, S.A., Carter, D.R.F., 2022. Utilising extracellular vesicles for early cancer diagnostics: benefits, challenges and recommendations for the future. Br. J. Cancer 126 (3), 323–330.

Puhka, M., Takatalo, M., Nordberg, M.-E., Valkonen, S., Nandania, J., Aatonen, M., Yliperttula, M., Laitinen, S., Velagapudi, V., Mirtti, T., Kallioniemi, O., Rannikko, A., Siljander, P.R.M., af Hällström, T.M., 2017. Metabolomic profiling of extracellular vesicles and alternative normalization methods reveal enriched metabolites and strategies to study prostate cancer-related changes. Theranostics 7 (16), 3824–3841.

Qiu, G., Zheng, G., Ge, M., Wang, J., Huang, R., Shu, Q., Xu, J., 2019. Functional proteins of mesenchymal stem cell-derived extracellular vesicles. Stem Cell Res. Ther. 10 (1), 359.

Reimhult, E., Kasemo, B., Höök, F., 2009. Rupture pathway of phosphatidylcholine liposomes on silicon dioxide. Int. J. Mol. Sci. 10 (4), 1683–1696.

Saito, M., Horie, S., Yasuhara, H., Kashimura, A., Sugiyama, E., Saijo, T., Mizuno, H., Kitajima, H., Todoroki, K., 2021. Metabolomic profiling of urine-derived extracellular vesicles from rat model of drug-induced acute kidney injury. Biochem. Biophys. Res. Commun. 546, 103–110.

Schapira, I., O'Neill, M.R., Russo-Savage, L., Narla, T., Laprade, K.A., Stafford, J.M., Ou, Y., 2023. Measuring tryptophan dynamics using fast scan cyclic voltammetry at carbon fiber microelectrodes with improved sensitivity and selectivity. RSC Adv. 13 (37), 26203–26212.

Taller, D., Richards, K., Slouka, Z., Senapati, S., Hill, R., Go, D.B., Chang, H.-C., 2015. On-chip surface acoustic wave lysis and ion-exchange nanomembrane detection of exosomal RNA for pancreatic cancer study and diagnosis. Lab Chip 15 (7), 1656–1666.

Théry, C., Witwer, K.W., Aikawa, E., Alcaraz, M.J., Anderson, J.D., Andriantsitohaina, R., Antoniou, A., Arab, T., Archer, F., Atkin-Smith, G.K., Ayre, D.C., Bach, J.M., Bachurski, D., Baharvand, H., Balaj, L., Baldacchino, S., Bauer, N.N., Baxter, A.A., Bebawy, M., Beckham, C., Bedina Zavec, A., Benmoussa, A., Berardi, A.C., Bergese, P., Bielska, E., Blenkiron, C., Bobis-Wozowicz, S., Boilard, E., Boireau, W., Bongiovanni, A., Borràs, F.E., Bosch, S., Boulanger, C.M., Breakefield, X., Breglio, A.M., Brennan, M., Brigstock, D.R., Brisson, A., Broekman, M.L., Bromberg, J.F., Bryl-Górecka, P., Buch, S., Buck, A.H., Burger, D., Busatto, S., Buschmann, D., Bussolati, B., Buzás, E.I., Byrd, J.B., Camussi, G., Carter, D.R., Caruso, S., Chamley, L.W., Chang, Y.T., Chen, C., Chen, S., Cheng, L., Chin, A.R., Clayton, A., Clerici, S.P., Cocks, A., Cocucci, E., Coffey, R.J., Cordeiro-da-Silva, A., Couch, Y., Coumans, F.A., Coyle, B., Crescitelli, R., Criado, M.F., D'Souza-Schorey, C., Das, S., Datta Chaudhuri, A., de Candia, P., De Santana, E.F., De Wever, O., Del Portillo, H.A., Demaret, T., Deville, S., Devitt, A., Dhondt, B., Di Vizio, D., Dieterich, L.C., Dolo, V., Dominguez Rubio, A.P., Dominici, M., Dourado, M.R., Driedonks, T.A., Duarte, F.V., Duncan, H.M., Eichenberger, R.M., Ekström, K., El Andaloussi, S., Elie-Caille, C., Erdbrügger, U., Falcón-Pérez, J.M., Fatima, F., Fish, J.E., Flores-Bellver, M., Försönits, A., Frelet-Barrand, A., Fricke, F., Fuhrmann, G., Gabrielsson, S., Gámez-Valero, A., Gardiner, C., Gärtner, K., Gaudin, R., Gho, Y.S., Giebel, B., Gilbert, C., Gimona, M., Giusti, I., Goberdhan, D.C., Görgens, A., Gorski, S.M., Greening, D.W., Gross, J.C., Gualerzi, A., Gupta, G.N., Gustafson, D., Handberg, A., Haraszti, R.A., Harrison, P., Hegyesi, H., Hendrix, A., Hill, A.F., Hochberg, F.H., Hoffmann, K.F., Holder, B., Holthofer, H., Hosseinkhani, B., Hu, G., Huang, Y., Huber, V., Hunt, S., Ibrahim, A.G., Ikezu, T., Inal, J.M., Isin, M., Ivanova, A., Jackson, H.K., Jacobsen, S., Jay, S.M., Jayachandran, M., Jenster, G., Jiang, L., Johnson, S.M., Jones, J.C., Jong, A., Jovanovic-Talisman, T., Jung, S., Kalluri, R., Kano, S.I., Kaur, S., Kawamura, Y., Keller, E.T., Khamari, D., Khomyakova, E., Khvorova, A., Kierulf, P., Kim, K.P., Kislinger, T., Klingeborn, M., Klinke 2nd, D.J., Kornek, M., Kosanović, M.M., Kovács Á, F., Krämer-Albers, E.M., Krasemann, S., Krause, M., Kurochkin, I.V., Kusuma, G.D., Kuypers, S., Laitinen, S., Langevin, S.M., Languino, L.R., Lannigan, J., Lässer, C., Laurent, L.C., Lavieu, G., Lázaro-Ibáñez, E., Le Lay, S., Lee, M.S., Lee, Y.X.F., Lemos, D.S., Lenassi, M., Leszczynska, A., Li, I.T., Liao, K., Libregts, S.F., Ligeti, E., Lim, R., Lim, S.K., Linē, A., Linnemannstöns, K., Llorente, A., Lombard, C.A., Lorenowicz, M.J., Lörincz Á, M., Lötvall, J., Lovett, J., Lowry, M.C., Loyer, X., Lu, Q., Lukomska, B., Lunavat, T.R., Maas, S.L., Malhi, H., Marcilla, A., Mariani, J., Mariscal, J., Martens-Uzunova, E.S., Martin-Jaular, L., Martinez, M.C., Martins, V.R., Mathieu, M., Mathivanan, S., Maugeri, M., McGinnis, L.K., McVey, M.J., Meckes Jr., D.G., Meehan, K.L., Mertens, I., Minciacchi, V.R., Möller, A., Møller Jørgensen, M., Morales-Kastresana, A., Morhayim, J., Mullier, F., Muraca, M., Musante, L., Mussack, V., Muth, D.C., Myburgh, K.H., Najrana, T., Nawaz, M., Nazarenko, I., Nejsum, P., Neri, C., Neri, T., Nieuwland, R., Nimrichter, L., Nolan, J.P., Nolte-'t Hoen, E.N., Noren Hooten, N., O'Driscoll, L., O'Grady, T., O'Loghlen, A., Ochiya, T., Olivier, M., Ortiz, A., Ortiz, L.A., Osteikoetxea, X., Østergaard, O., Ostrowski, M., Park, J., Pegtel, D.M., Peinado, H., Perut, F., Pfaffl, M.W., Phinney, D.G., Pieters, B.C., Pink, R.C., Pisetsky, D.S., Pogge von Strandmann, E., Polakovicova, I., Poon, I.K., Powell, B.H., Prada, I., Pulliam, L., Quesenberry, P., Radeghieri, A., Raffai, R.L., Raimondo, S., Rak, J., Ramirez, M.I., Raposo, G.,

Rayyan, M.S., Regev-Rudzki, N., Ricklefs, F.L., Robbins, P.D., Roberts, D.D., Rodrigues, S.C., Rohde, E., Rome, S., Rouschop, K.M., Rughetti, A., Russell, A.E., Saá, P., Sahoo, S., Salas-Huenuleo, E., Sánchez, C., Saugstad, J.A., Saul, M.J., Schiffelers, R.M., Schneider, R., Schøyen, T.H., Scott, A., Shahaj, E., Sharma, S., Shatnyeva, O., Shekari, F., Shelke, G.V., Shetty, A.K., Shiba, K., Siljander, P.R., Silva, A.M., Skowronek, A., Snyder 2nd, O.L., Soares, R.P., Sódar, B.W., Soekmadji, C., Sotillo, J., Stahl, P.D., Stoorvogel, W., Stott, S.L., Strasser, E.F., Swift, S., Tahara, H., Tewari, M., Timms, K., Tiwari, S., Tixeira, R., Tkach, M., Toh, W.S., Tomasini, R., Torrecilhas, A.C., Tosar, J.P., Toxavidis, V., Urbanelli, L., Vader, P., van Balkom, B.W., van der Grein, S.G., Van Deun, J., van Herwijnen, M.J., Van Keuren-Jensen, K., van Niel, G., van Royen, M.E., van Wijnen, A.J., Vasconcelos, M.H., Vechetti Jr., I.J., Veit, T.D., Vella, L.J., Velot, É., Verweij, F.J., Vestad, B., Viñas, J.L., Visnovitz, T., Vukman, K.V., Wahlgren, J., Watson, D.C., Wauben, M.H., Weaver, A., Webber, J.P., Weber, V., Wehman, A.M., Weiss, D.J., Welsh, J.A., Wendt, S., Wheelock, A.M., Wiener, Z., Witte, L., Wolfram, J., Xagorari, A., Xander, P., Xu, J., Yan, X., Yáñez-Mó, M., Yin, H., Yuana, Y., Zappulli, V., Zarubova, J., Žėkas, V., Zhang, J.Y., Zhao, Z., Zheng, L., Zheutlin, A.R., Zickler, A.M., Zimmermann, P., Zivkovic, A.M., Zocco, D., Zuba-Surma, E.K., 2018. Minimal information for studies of extracellular vesicles 2018 (MISEV2018): a position statement of the International Society for Extracellular Vesicles and update of the MISEV2014 guidelines. J. Extracell. Vesicles 7 (1), 1535750.

Wang, X., Huang, J., Chen, W., Li, G., Li, Z., Lei, J., 2022. The updated role of exosomal proteins in the diagnosis, prognosis, and treatment of cancer. Exp. Mol. Med. 54 (9), 1390–1400.

Welsh, J.A., Arkesteijn, G.J.A., Bremer, M., Cimorelli, M., Dignat-George, F., Giebel, B., Görgens, A., Hendrix, A., Kuiper, M., Lacroix, R., Lannigan, J., van Leeuwen, T.G., Lozano-Andrés, E., Rao, S., Robert, S., de Rond, L., Tang, V.A., Tertel, T., Yan, X., Wauben, M.H.M., Nolan, J.P., Jones, J.C., Nieuwland, R., van der Pol, E., 2023. A compendium of single extracellular vesicle flow cytometry. J. Extracell. Vesicles 12 (2), e12299.

Yadav, S., Boriachek, K., Islam, M.N., Lobb, R., Möller, A., Hill, M.M., Hossain, M.S.A., Nguyen, N.-T., Shiddiky, M.J.A., 2017. An electrochemical method for the detection of disease-specific exosomes. Chemelectrochem 4 (4), 967–971.

Yu, W., Hurley, J., Roberts, D., Chakrabortty, S.K., Enderle, D., Noerholm, M., Breakefield, X.O., Skog, J.K., 2021. Exosome-based liquid biopsies in cancer: opportunities and challenges. Ann. Oncol. 32 (4), 466–477.

Zhang, W., Tian, Z., Yang, S., Rich, J., Zhao, S., Klingeborn, M., Huang, P.-H., Li, Z., Stout, A., Murphy, Q., Patz, E., Zhang, S., Liu, G., Huang, T.J., 2021. Electrochemical micro-aptasensors for exosome detection based on hybridization chain reaction amplification. Microsystems & Nanoengineering 7 (1), 63.

Zhang, Y., Li, M., Li, Z., Li, Q., Aldalbahi, A., Shi, J., Wang, L., Fan, C., Zuo, X., 2017. Recognizing single phospholipid vesicle collisions on carbon fiber nanoelectrode. Sci. China Chem. 60 (11), 1474–1480.

Zhou, Q., Rahimian, A., Son, K., Shin, D.-S., Patel, T., Revzin, A., 2016. Development of an aptasensor for electrochemical detection of exosomes. Methods 97, 88–93.

Zhu, Y., An, Y., Li, R., Zhang, F., Wang, Q., He, P., 2020. Double imprinting-based electrochemical detection of mimetic exosomes. J. Electroanal. Chem. 862, 113969.